Nanoscale

COMMUNICATION

View Article Online
View Journal | View Issue

Cite this: *Nanoscale*, 2014, **6**, 5087

Received 10th December 2013
Accepted 19th February 2014

DOI: 10.1039/c3nr06539a

www.rsc.org/nanoscale

Carbon dioxide conversion into hydrocarbon fuels on defective graphene-supported Cu nanoparticles from first principles†

Dong-Hee Lim,*[ab] Jun Ho Jo,[a] Dong Yun Shin,[a] Jennifer Wilcox,[c] Hyung Chul Ham[a] and Suk Woo Nam[a]

Density functional theory studies demonstrate that defective graphene-supported Cu nanoparticles can modify the structural and electronic properties of copper for enhancing electrochemical reduction of carbon dioxide (CO_2) into hydrocarbon fuels (CH_4, CO, and HCOOH). We not only provide improved understanding of CO_2 conversion mechanisms on both Cu and the Cu nanoparticle system, but also explain a key factor for enhanced CO_2 conversion. A promising catalytic material for CO_2 conversion into hydrocarbon fuels may allow for geometry flexibility upon interaction with a key intermediate of CHO*.

The electrochemical conversion of CO_2 to hydrocarbon fuels would not only assist in paving a path toward renewable energy, but also contribute to mitigating CO_2 emissions. The main challenge for advancing CO_2 reduction is to improve the energy efficiency of the process. Although both reasonably high current densities and moderate efficiencies have been achieved, they have not yet been achieved together.[1] Various metal-based catalysts (*i.e.*, copper,[2–4] platinum,[5,6] iron,[7,8] nickel,[9,10] gold[11–13]) have been used to improve energy efficiency of the electrochemical reduction of CO_2. Among them, copper has been widely accepted as a promising metal for CO_2 reduction due to its high ability to produce hydrocarbon fuels such as carbon monoxide (CO), formic acid (HCOOH), methane (CH_4), and ethane (C_2H_4)[3]; however, the quantities of produced fuels are inefficient due to the large overpotential. According to experiments[14] and density functional theory (DFT) modeling investigations,[15] the production of CH_4 from CO_2 requires at least −0.8 V *vs.* RHE (*i.e.*, reversible hydrogen electrode, in which the measured potential does not change with the pH). Hori *et al.*[14] pointed out that the electrochemical reduction of CO_2 is primarily hindered by a high overpotential, which results from the initial electron transfer to form the intermediate species, $^{\bullet}CO_2^{-}$. Also, recent DFT studies of CO_2 electrochemical reduction have used CO and CHO intermediates as activity descriptors for CO_2 reduction to methane,[15–17] which is based on the fact that previous experimental studies[18–20] demonstrated that CO adsorption dominates on the electrode surface during CO_2 reduction.

Peterson *et al.*[15,16] demonstrated by conducting DFT studies that the key step in controlling the formation of hydrocarbons in the electrochemical reduction of CO_2 is the protonation of adsorbed CO* to form the adsorbed CHO* intermediate (where "*" denotes the adsorbed species and will be referred to as such hereafter). By increasing the stability of the CHO* species relative to CO*, it is expected that the energy efficiency of the electrochemical reduction of CO_2 would increase due to a significantly lowered overpotential. This may be achieved by utilizing nanostructures of copper supported on graphene. Changes in the lattice constant, surface stress and surface energy associated with the nanoparticle size may improve the surface activity of copper for CO_2 reduction. Additionally, the unique electronic and physical properties of graphene would improve the CO_2 reduction kinetics, as it has been previously shown that graphene can enhance reaction kinetics on noble metal nanoparticles.[21–25] Also, carbon vacancies in graphene may significantly influence its physical and chemical characteristics and magnetic properties[26–30] and can be used as anchoring points for the growth of metal nanoparticles, which will increase the durability of the Cu nanoparticle–graphene system and prevent sintering of the Cu nanoparticles.

The current communication discusses improved catalysts for electrochemical CO_2 reduction to hydrocarbon fuels on Cu nanoparticles anchored at carbon vacancy sites of graphene. For this, free energies of the CO_2 reduction intermediates in

[a]*Fuel Cell Research Center, Korea Institute of Science and Technology (KIST), Hwarangno 14-gil 5, Seongbuk-gu, Seoul 136-791, Republic of Korea. E-mail: limkr@kist.re.kr; galer821@gmail.com; 84sindy@gmail.com; hchahm@kist.re.kr; swn@kist.re.kr; Fax: +82-2-958-5199; Tel: +82-2-958-5293*

[b]*Department of Environmental Engineering, Chungbuk National University 52 Naesudong-ro, Heungdeok-gu, Cheongju, Chungbuk 361-763, Republic of Korea. E-mail: wilcoxj@stanford.edu*

[c]*Department of Energy Resources Engineering, Stanford University, 367 Panama Street, Green Earth Sciences, Stanford, CA 94305-2220, USA. E-mail: wilcoxj@stanford.edu*

† Electronic supplementary information (ESI) available. See DOI: 10.1039/c3nr06539a

electrochemical reaction pathways were calculated by using density functional theory (DFT) coupled with a computational hydrogen electrode (CHE) model suggested by Nørskov *et al.*[15,31] Electron exchange–correlation functionals were represented with the generalized gradient approximation (GGA), and the model of Perdew, Burke and Ernzerhof (PBE)[32] was used for the nonlocal corrections. By employing the CHE model, a proton/electron ($H^+ + e^-$) in solution can be indirectly treated and the effect of a bias can be applied by shifting ΔG by $+neU$, where n is the number of proton–electron pairs transferred, e is the elementary positive charge, and U is the applied potential. The free energy change (ΔG) is calculated as $\Delta G = \Delta E + \Delta ZPE - T\Delta S$, where ΔE is the total energy change directly obtained from DFT calculations, ΔZPE is the change in zero-point energies, T is temperature, and ΔS is the change in entropy. The temperature is set to 18.5 °C to compare current DFT results with the experimental data of Hori *et al.*[3] Details of the free energy calculations including DFT total energies, ZPE, entropies, and free energies of the intermediates and the solvation energy correction are described in ESI Section 1.†

Fig. 1 depicts the Cu nanoparticle–graphene system consisting of an icosahedral Cu_{55} nanoparticle (diameter of ~0.9 nm) adsorbed onto a 5-8-5 vacancy site of graphene (70 carbon atoms), which is motivated by the magic numbers (13, 55, 147, *etc.*)[33,34] of transition metal clusters providing a higher geometric or electronic stability compared to other cluster sizes. The Cu_{55} nanoparticle shows a strong DFT adsorption energy of −4.26 eV, in which Cu is interacting with the dangling bonds of the neighboring carbons near the 5-8-5 vacancy site, which implies that the strong interaction may help to prevent sintering of the Cu nanoparticles. The size of the Cu nanoparticle used in the DFT calculations is smaller than those conventionally synthesized experimentally; however, considering the limitation of DFT calculations in terms of the system size that can be efficiently treated, Cu_{55} is adequately large thereby minimizing the strong binding effect associated with highly undercoordinated Cu atoms that cause unrealistically high reactivity, thereby leading to an overestimation of overpotentials as was previously discussed in the work by Lim and Wilcox on the oxygen reduction reaction on Pt_{13}-defective graphene.[29,30] In addition, the Cu nanoparticle size (~0.9 nm) may be plausible in electrochemical experiments as demonstrated in oxygen reduction reactions on graphene supported-gold clusters with diameters of approximately 1–2.5 nm (an average diameter of 1.8 nm)[35] and on graphene quantum dots-supported platinum nanoparticles with diameters of 2.2–3.3 nm (an average diameter of 2.8 nm).[36]

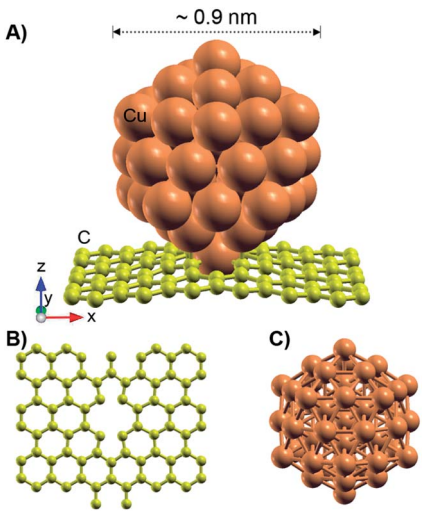

Fig. 1 (A) Side view of a Cu_{55} nanoparticle supported on defective graphene. (B) Top view of a 5-8-5 vacancy site of defective graphene with two missing C atoms at its center. (C) Icosahedral Cu_{55} nanoparticle. Brown and yellow colors represent Cu and C, respectively.

Fig. 2 shows the lowest energy pathways of CO_2 reduction on the Cu_{55}–defective graphene surface and a comparison of the CO_2 reduction mechanisms between the Cu(111) (*i.e.*, the most stable flat Cu surface among (100), (110), and (111) faces) and the Cu_{55}–defective graphene surfaces. Peterson *et al.*[15] extensively investigated the electroreduction of CO_2 on a Cu(211) surface and determined the lowest energy intermediates. Based on this, we have examined three possible adsorption configurations for each intermediate and determined the lowest energy pathways as shown in Fig. 2A. By transferring ($H^+ + e^-$) from solution to an adsorbed species, a gas-phase CO_2 molecule is converted to COOH* → CO* → CHO* → CH_2O* → CH_3O* → O* → OH* → H_2O_{gas}. The reaction intermediate configurations on the Cu(111) surface are also similar to those of Fig. 2A (data not shown here).

At zero electrode potential ($U = 0$ V) in Fig. 2B, the Cu(111) surface shows a key energy barrier of 0.97 eV required for the protonation step of the CO species (CO* → CHO*: (2) → (3) in Fig. 2B). This agrees reasonably well with the protonation step barrier of 0.74 eV on the Cu(211) step surface conducted by Peterson *et al.*,[15] which is due to the fact that a step-like surface of Cu(211) is more reactive toward binding adsorbates than a flat surface. In the Cu_{55}–defective graphene system, reaction across the uncoordinated site significantly lowers the energy barrier of the key potential-limiting step to 0.68 eV; in other words, CHO* becomes more stabilized relative to CO* on the Cu_{55}–defective graphene surface compared to on the Cu(111) surface. This implies that the Cu_{55}–defective graphene system may help enhance the energy efficiency of the electrochemical reduction of CO_2 by lowering the key energy barrier. Instead, the Cu_{55}–defective graphene system may hinder further reaction steps toward oxygen reduction due to an increased energy barrier associated with the proton/electron-transfer step of OH* between steps (7) and (8) (*i.e.*, OH* → H_2O) in Fig. 2B. For this step, the Cu(111) surface requires 0.39 eV, while the Cu_{55}–defective graphene system requires 0.60 eV. Considering the endothermic reaction steps of both systems in Fig. 2B, the rate-limiting steps of the CO_2 reduction on the Cu(111) surface and Cu_{55}–defective graphene system lie in the CO* → CHO* step.

Fig. 2C shows the CO_2 reduction mechanisms at applied electrode potentials of $U = -0.97$ and −0.68 V for the Cu(111) surface and the Cu_{55}–defective graphene system, respectively. The applied potentials are required voltages for eliminating the energy barriers of the rate-limiting step (CO* → CHO*), which shows that the hydrocarbon CH_4-forming reaction from CO_2

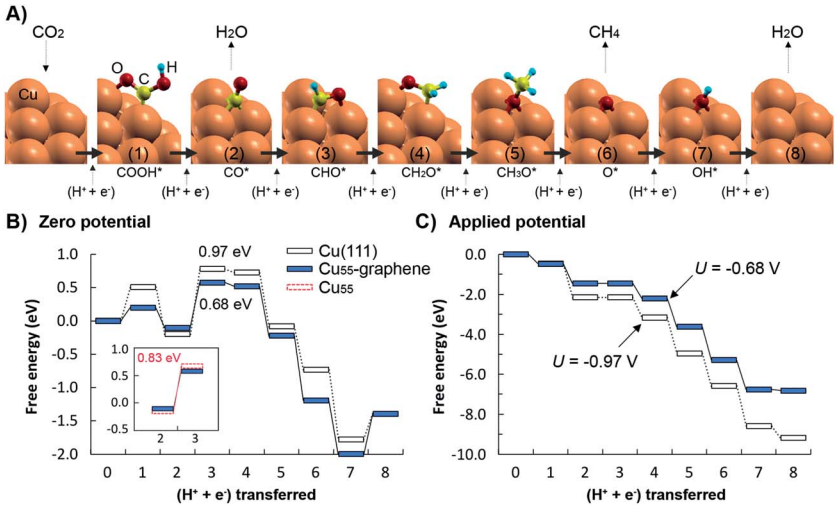

Fig. 2 (A) The lowest energy pathways of CO_2 reduction on the Cu_{55}–defective graphene. (B and C) Relative free energy diagrams without (B) and with (C) applied potential for CO_2 reduction on Cu(111) (empty rectangle with dashed lines), Cu_{55}–defective graphene (filled rectangle with solid lines), and Cu_{55} cluster (empty rectangle in the inset).

may occur at −0.97 and −0.68 V (*vs.* RHE) on the Cu(111) surface and the Cu_{55}–defective graphene system, respectively. The DFT potential of −0.97 V on the Cu(111) surface agrees fairly well with experimental measurements, in which the formation of CH_4 from CO_2 on copper is initiated at about −0.8 V and is maximized at about −1.0 V at 18.5 °C.[3,15] An interesting finding is that the Cu_{55}–defective graphene system requires approximately 30% less potential compared to the planar Cu(111) surface. Details of the CO_2 reduction reactions and free energy data are shown in ESI Section 2.†

To understand in greater detail the reason for the smaller potential required for CH_4 formation on the Cu_{55}–defective graphene system, the projected density of states (PDOS) of CO*, CHO*, and surface Cu atoms neighboring the adsorbates were analyzed by decomposing the electron density and wave function into the atomic orbital contributions. In Fig. 3A, the Cu(111) surfaces with CO* and CHO* show hybridized s-, p-, and d-orbitals of Cu with s- and p-orbitals of the adsorbates between −6 and −12 eV. This phenomenon is also similarly shown in the case of the Cu_{55}–defective graphene systems as indicated in Fig. 3B. Both surface systems show strongly hybridized orbitals when CO is adsorbed; however, when CHO is adsorbed, the Cu(111) surface with the CHO* intermediate species indicates relatively weaker hybridization while the Cu_{55}–defective graphene system with CHO* shows stronger hybridization between −8 and −6 eV and near the edge of the valence zone. This greater CHO–Cu overlap population on the Cu nanoparticle represents a relatively stronger stabilization of the CHO species on the Cu_{55}–defective graphene system compared to the Cu(111) surface. Full details of each PDOS are shown in ESI Section 3.†

The stronger orbital hybridization between Cu and CHO on the Cu_{55}–defective graphene system may be attributed to the advantage associated with graphene's unique electronic and physical properties as previously discussed. To confirm this, the key potential limiting step of CO* → CHO* was examined on a Cu_{55} cluster without graphene as shown in the inset of Fig. 2B. Without the graphene support, the energy barrier of the key step is 0.78 eV, demonstrating that the graphene support contributes to lowering the energy barrier of the key step from 0.83 to

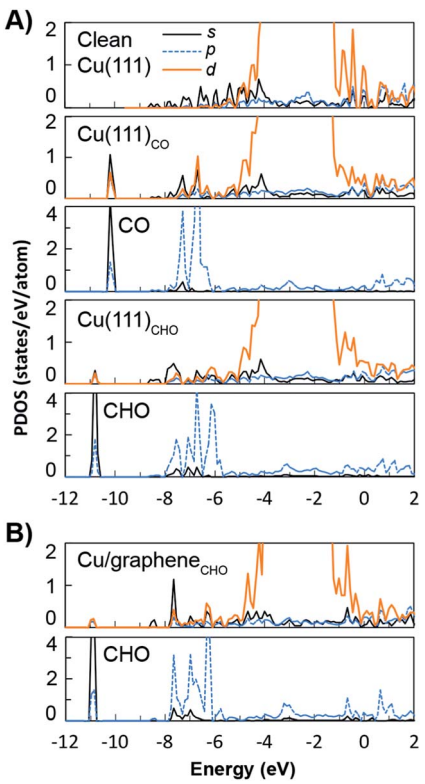

Fig. 3 Projected density of states (PDOS) of the Cu(111) surface with adsorbed CO and CHO (A) and the Cu_{55}–graphene surface with CHO (B). A system title of X_Y indicates a surface (X) with adsorbed species (Y). Clean Cu, CO, and CHO represent clean Cu(111), adsorbed CO, and adsorbed CHO, respectively. The Fermi energy is referenced at 0 eV.

0.68 eV by modifying the electron properties of the anchored Cu_{55}. To better understand this, the d-band centers of Cu atoms were calculated. The d-band centers of all Cu atoms (or two Cu atoms where CHO* is adsorbed) of the Cu_{55} cluster and the Cu_{55}–defective graphene are −2.24 (or −2.10) and −2.17 (or −2.07) eV, respectively. The higher shift of the d-band centers of the Cu_{55}–defective graphene toward the Fermi level indicates the higher reactivity of Cu atoms resulting in an increase in the stability of adsorbates, which is attributed to the fact that an upshift of the d-band center causes the antibonding orbitals to shift higher, potentially making them more difficult to fill.

Also, another important factor for the stronger orbital hybridization between Cu and CHO on the Cu_{55}–defective graphene system may be the geometry flexibility of the Cu nanoparticle. The geometry of the Cu nanoparticle is more flexible than that of the Cu(111) surface, which promotes CHO binding on the Cu nanoparticle by increasing the Cu–Cu distance when the CHO* species is formed on the Cu nanoparticle surface. This is supported by the Cu–Cu distance measured at the CHO adsorbed site across both systems. The Cu–Cu distance of the Cu_{55}–defective graphene system increases from 2.584 to 2.895 Å (12.1% increase), while that of the Cu(111) surface is expanded from 2.571 to 2.683 Å (4.4% increase) (see ESI Section 4†). In other words, the geometry flexibility of the Cu nanoparticle has locally caused an expansive lattice strain effect, which in turn strengthens the Cu interaction with CHO species. This kind of strain effect is well known in metals or metal alloys, where an expansion in the lattice parameter can induce a shift in the d-band interaction toward the Fermi energy, resulting in strengthening the adsorbate interaction on catalytic surfaces.[37] Sakong and Gross[38] reported that the lattice expansive strain of copper surfaces (Cu(100), Cu(110), and Cu(111)) causes an upshift in the d-band centers. On the other hand, electronic ligand effects induced by the modification of electronic properties may have a minimal effect on the stability of the CHO* intermediate species on both systems. This is because the PDOS of both clean systems are not significantly different, as shown in ESI Section 3.†

Furthermore, the reaction pathways toward the production of formic acid (HCOOH) and carbon monoxide (CO) gases are shown in Fig. 4. HCOOH and CO gases are produced when the second proton and electron (*i.e.*, $H^+ + e^-$) are transferred at steps 2(a) and 2(b) in Fig. 4A and B, respectively. On the Cu(111) surface, the formation of both HCOOH and CO requires a potential of −0.51 V, by which the potential-limiting energy barriers at the first $H^+ + e^-$ step are eliminated. This is in agreement with previous experiments[14] in addition to previous DFT studies[15,16] where the formation of HCOOH and CO gases requires about −0.4 to −0.5 V (*vs.* RHE). The COOH* species is more stable on the Cu_{55}–defective graphene system compared to the Cu(111) surface for a similar reason as discussed previously with regard to the flexibility of the Cu nanoparticle geometry, resulting in limiting potentials of −0.19 and −0.39 V for the production of HCOOH and CO gases, respectively. This lower overpotential on the Cu_{55}–defective graphene system may lead to the higher selectivity of HCOOH and CO compared to that on the Cu(111) surface.

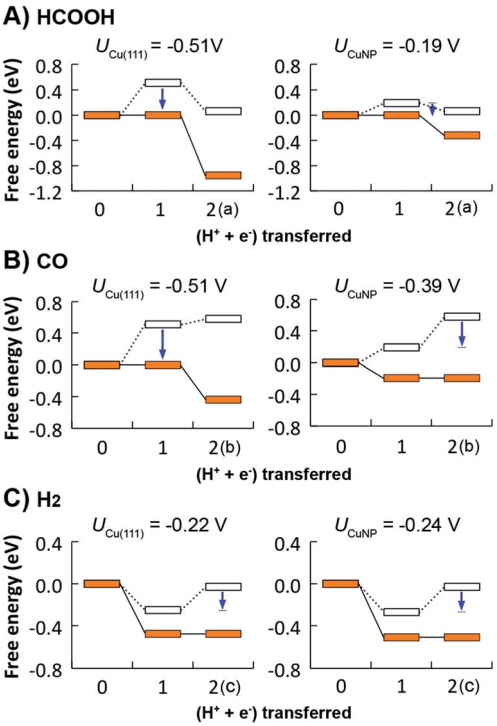

Fig. 4 Relative free energy diagrams for HCOOH (A), CO (B), and H_2 (C) gas production on Cu(111) (left) and Cu_{55}–defective graphene (right). Empty rectangles (with dashed lines) and filled rectangles (with solid lines) represent reactions without and with applied potentials. ($H^+ + e^-$) transferred steps of 0 and 1 are the same steps as shown in Fig. 2. The steps of 2(a), 2(b), and 2(c) represent $HCOOH_{(gas)}$ + surface, $CO_{(gas)} + H_2O_{(gas)}$ + surface, and $H_{2(gas)}$ + surface, respectively. $U_{Cu(111)}$ and U_{CuNP} indicate necessary potentials to produce the gases on Cu(111) and Cu_{55}–defective graphene, respectively. Arrows show the potential-limiting energy barriers that should be overcome for the gas production.

In addition to the key rate-limiting steps of the protonation of adsorbed CO (CO* → CHO*) in CO_2 reduction, the hydrogen evolution reaction (HER) significantly affects the electrochemical reduction of CO_2 since HER is competitive against CO_2 reduction. Effective CO_2 reduction catalysts should show poor activity for the competitive HER.[15–17] In terms of the selectivity of H_2 gas production, the Cu_{55}–defective graphene system shows a slightly poor activity for HER compared to the Cu(111) system as shown in Fig. 4C, indicating limiting potentials of −0.22 and −0.24 V on the Cu(111) and Cu_{55}–defective graphene surfaces, respectively. In both cases, the potential limiting barriers for HER are present in the H_2 gas desorption step ($H^* + H \rightarrow H_{2(gas)}$), which is attributed to the fact that atomic hydrogen adsorption is exothermic and its desorption is endothermic. The adsorption free energies of atomic hydrogen on the Cu(111) surface and Cu_{55}–defective graphene surfaces are −0.30 and −0.32 eV, respectively, which are comparative to the atomic hydrogen adsorption energy of −0.18 eV on the Cu(111) surface[17] calculated using the GGA-PW91 functional. The predicted potential limiting step for HER in the current work agrees with previous DFT studies using a PBE functional and showing a potential of −0.1 V on the Cu(211) step

surface,[15,17] but the magnitude is different due to the stronger hydrogen adsorption at the fcc hollow sites of the Cu(111) surface. Note that the potential limiting step for HER may vary slightly depending on the DFT functional; for example, Peterson *et al.*'s work using the revised PBE (RPBE) functional suggests a limiting potential of −0.03 V due to an endothermic adsorption of atomic hydrogen on the Cu(211) step site.[15] Nevertheless, we may conclude from Fig. 4 that the Cu_{55}–defective graphene system promotes CO_2 reduction into hydrocarbon fuels by lowering the rate-limiting energy barriers and relatively slightly inhibiting HER, at least showing similar selectivity of H_2 compared to the Cu(111) surface.

Lastly, it is worth noting the solvation effect in DFT modeling. Since an explicit treatment of a number of water molecules is still difficult to carry out using DFT, indirect methods may provide insight into better understanding the solvation effect. According to Peterson *et al.*'s solvation energy approximation on flat metal surfaces,[15,31,39] OH*, R–OH*, CO*, and CHO* gas-phase adsorbates may be stabilized in liquid water by approximately 0.5, 0.25, 0.1, and 0.1 eV, respectively. The current work employs this simple approximation for the adsorbed species and uses chemical potentials of the gas-phase molecules calculated in the work of Peterson *et al.*[15] where standard ideal-gas methods[40] were used to convert electronic energies of gas-phase molecules into chemical potentials at 18.5 °C (*e.g.*, the free energy of liquid water was calculated as an ideal gas and adjusted to a fugacity of 3534 Pa, which is the vapor pressure of water) (see ESI Section 1†). If the solvation correction is not considered, the energy barrier of the first $H^+ + e^-$ transfer step (*i.e.*, $CO_2 \rightarrow COOH^*$) is overestimated resulting in the required potential of −0.76 V for the HCOOH and CO formation on the Cu(111) surface, which does not agree with the experimental observation (between −0.4 and −0.5 V).[3] Overall, the solvation energy correction lowers the reaction energy states and the reaction energy barriers become smaller; however, the relatively large solvation energy of OH* causes an increase in the energy barrier for H_2O desorption. In other words, the desorption energy of H_2O from catalytic surfaces may be underestimated if the solvation effect is not taken into account. A detailed comparison between with and without solvation is provided in ESI Section 5.†

Conclusions

The current work provides theoretical evidence for improved CO_2 conversion into hydrocarbon fuels by using defective graphene-supported Cu nanoparticles. The results imply that an alternative catalytic material that allows for geometry flexibility upon interaction with adsorbates, especially with CHO*, may improve CO_2 conversion into hydrocarbon fuels. A promising material may be Cu nanoparticles supported on defective graphene as demonstrated here. In addition to the benefits of Cu nanoparticles, the defective graphene support may not only promote electron transport to the key potential limiting step species of CHO*, but also help prevent sintering of Cu nanoparticles due to the strong anchoring nature of its defect sites. An improved understanding of CO_2 conversion mechanisms and the key factor regarding the geometry flexibility for the enhanced CO_2 conversion may help design promising materials for CO_2 conversion into hydrocarbon fuels. Also, future studies may need to focus on improving our understanding of solvation energies of COOH* species showing the influence on HCOOH and CO gas production and its selectivity.

Acknowledgements

The current work is supported by the Basic Science Research Program through the National Research Foundation (NRF) of Korea funded by the Ministry of Education, Science and Technology (2012R1A6A3A04040490) and by the Supercomputing Center/Korea Institute of Science and Technology Information with supercomputing resources including technical support (KSC-2013-C3-017).

Notes and references

1 D. T. Whipple and P. J. A. Kenis, Prospects of CO_2 Utilization *via* Direct Heterogeneous Electrochemical Reduction, *J. Phys. Chem. Lett.*, 2010, **1**(24), 3451–3458.
2 Y. Hori, K. Kikuchi, A. Murata and S. Suzuki, Production of methane and ethylene in electrochemical reduction of carbon dioxide at copper electrode in aqueous hydrogencarbonate solution, *Chem. Lett.*, 1986, **15**, 897–898.
3 Y. Hori, A. Murata and R. Takahashi, Formation of Hydrocarbons in the Electrochemical Reduction of Carbon-Dioxide at a Copper Electrode in Aqueous-Solution, *J. Chem. Soc., Faraday Trans. 1*, 1989, **85**, 2309–2326.
4 D. W. Dewulf, T. Jin and A. J. Bard, Electrochemical and surface studies of carbon-dioxide reduction to methane and ethylene at copper electrodes in aqueous-solutions, *J. Electrochem. Soc.*, 1989, **136**(6), 1686–1691.
5 S. G. Sun and Z. Y. Zhou, Surface processes and kinetics of CO_2 reduction on Pt(100) electrodes of different surface structure in sulfuric acid solutions, *Phys. Chem. Chem. Phys.*, 2001, **3**(16), 3277–3283.
6 I. Kerbach, V. Climent and J. M. Feliu, Reduction of CO_2 on bismuth modified Pt(1 1 0) single-crystal surfaces. Effect of bismuth and poisoning intermediates on the rate of hydrogen evolution, *Electrochim. Acta*, 2011, **56**(12), 4451–4456.
7 H. Takahashi, L. H. Liu, Y. Yashiro, K. Ioku, G. Bignall, N. Yamasaki and T. Kori, CO_2 reduction using hydrothermal method for the selective formation of organic compounds, *J. Mater. Sci.*, 2006, **41**(5), 1585–1589.
8 G. Q. Guan, T. Kida, T. Ma, K. Kimura, E. Abe and A. Yoshida, Reduction of aqueous CO_2 at ambient temperature using zero-valent iron-based composites, *Green Chem.*, 2003, **5**(5), 630–634.
9 D. J. Pearce and D. Pletcher, A study of the mechanism for the electrocatalysis of carbon-dioxide reduction by nickel and cobalt square-planar complexes in solution, *J. Electroanal. Chem.*, 1986, **197**(1–2), 317–330.
10 E. Y. Lee, D. W. Hong, H. W. Park and M. P. Suh, Synthesis, properties, and reactions of trinuclear macrocyclic nickel(II)

and nickel(I) complexes: Electrocatalytic reduction of CO_2 by nickel(II) complex, *Eur. J. Inorg. Chem.*, 2003, **17**, 3242–3249.
11 Y. Hori, K. Kikuchi and S. Suzuki, Production of CO and CH_4 in electrochemical reduction of CO_2 at metal-electrodes in aqueous hydrogencarbonate solution, *Chem. Lett.*, 1985, **11**, 1695–1698.
12 T. Ohmori, A. Nakayama, H. Mametsuka and E. Suzuki, Influence of sputtering parameters on electrochemical CO_2 reduction in sputtered Au electrode, *J. Electroanal. Chem.*, 2001, **514**(1–2), 51–55.
13 G. B. Stevens, T. Reda and B. Raguse, Energy storage by the electrochemical reduction of CO_2 to CO at a porous Au film, *J. Electroanal. Chem.*, 2002, **526**(1–2), 125–133.
14 Y. Hori, H. Wakebe, T. Tsukamoto and O. Koga, Electrocatalytic process of CO selectivity in electrochemical reduction of CO_2 at metal-electrodes in aqueous-media, *Electrochim. Acta*, 1994, **39**(11–12), 1833–1839.
15 A. A. Peterson, F. Abild-Pedersen, F. Studt, J. Rossmeisl and J. K. Nørskov, How copper catalyzes the electroreduction of carbon dioxide into hydrocarbon fuels, *Energy Environ. Sci.*, 2010, **3**(9), 1311–1315.
16 A. A. Peterson and J. K. Nørskov, Activity descriptors for CO_2 electroreduction to methane on transition-metal catalysts, *J. Phys. Chem. Lett.*, 2012, **3**(2), 251–258.
17 P. Hirunsit, Electroreduction of Carbon Dioxide to Methane on Copper, Copper–Silver, and Copper–Gold Catalysts: A DFT Study, *J. Phys. Chem. C*, 2013, **117**(16), 8262–8268.
18 B. D. Smith, D. E. Irish, P. Kedzierzawski and J. Augustynski, A surface enhanced Raman scattering study of the intermediate and poisoning species formed during the electrochemical reduction of CO_2 on copper, *J. Electrochem. Soc.*, 1997, **144**(12), 4288–4296.
19 Y. Ichinohe, T. Wadayama and A. Hatta, Electrochemical reduction of CO_2 on silver as probed by surface-enhanced Raman scattering, *J. Raman Spectrosc.*, 1995, **26**(5), 335–340.
20 A. J. McQuillan, P. J. Hendra and M. Fleischmann, Raman spectroscopic investigation of silver electrodes, *J. Electroanal. Chem.*, 1975, **65**(2), 933–944.
21 R. Kou, Y. Shao, D. Wang, M. H. Engelhard, J. H. Kwak, J. Wang, V. V. Viswanathan, C. Wang, Y. Lin, Y. Wang, I. A. Aksay and J. Liu, Enhanced activity and stability of Pt catalysts on functionalized graphene sheets for electrocatalytic oxygen reduction, *Electrochem. Commun.*, 2009, **11**(5), 954–957.
22 B. Seger and P. V. Kamat, Electrocatalytically active graphene–platinum nanocomposites. Role of 2-D carbon support in PEM fuel cells, *J. Phys. Chem. C*, 2009, **113**(19), 7990–7995.
23 C. V. Rao, A. L. M. Reddy, Y. Ishikawa and P. M. Ajayan, Synthesis and electrocatalytic oxygen reduction activity of graphene-supported Pt_3Co and Pt_3Cr alloy nanoparticles, *Carbon*, 2011, **49**(3), 931–936.
24 M. H. Seo, S. M. Choi, H. J. Kim and W. B. Kim, The graphene-supported Pd and Pt catalysts for highly active oxygen reduction reaction in an alkaline condition, *Electrochem. Commun.*, 2011, **13**(2), 182–185.
25 E. Yoo, T. Okata, T. Akita, M. Kohyama, J. Nakamura and I. Honma, Enhanced electrocatalytic activity of Pt subnanoclusters on graphene nanosheet surface, *Nano Lett.*, 2009, **9**(6), 2255–2259.
26 J. M. Carlsson and M. Scheffler, Structural, electronic, and chemical properties of nanoporous carbon, *Phys. Rev. Lett.*, 2006, **96**(4), 046806.
27 Y. Ma, P. O. Lehtinen, A. S. Foster and R. M. Nieminen, Magnetic properties of vacancies in graphene and single-walled carbon nanotubes, *New J. Phys.*, 2004, **6**(68), 68.
28 D.-H. Lim, A. S. Negreira and J. Wilcox, DFT studies on the interaction of defective graphene-supported Fe and Al nanoparticles, *J. Phys. Chem. C*, 2011, **115**(18), 8961–8970.
29 D.-H. Lim and J. Wilcox, DFT-based study on oxygen adsorption on defective graphene-supported Pt nanoparticles, *J. Phys. Chem. C*, 2011, **115**(46), 22742–22747.
30 D. H. Lim and J. Wilcox, Mechanisms of the Oxygen Reduction Reaction on Defective Graphene-Supported Pt Nanoparticles from First-Principles, *J. Phys. Chem. C*, 2012, **116**(5), 3653–3660.
31 J. K. Nørskov, J. Rossmeisl, A. Logadottir, L. Lindqvist, J. R. Kitchin, T. Bligaard and H. Jónsson, Origin of the overpotential for oxygen reduction at a fuel-cell cathode, *J. Phys. Chem. B*, 2004, **108**(46), 17886–17892.
32 J. P. Perdew, K. Burke and M. Ernzerhof, Generalized gradient approximation made simple, *Phys. Rev. Lett.*, 1996, **77**(18), 3865–3868.
33 M. Sakurai, K. Watanabe, K. Sumiyama and K. Suzuki, Magic numbers in transition metal (Fe, Ti, Zr, Nb, and Ta) clusters observed by time-of-flight mass spectrometry, *J. Chem. Phys.*, 1999, **111**(1), 235–238.
34 L. Lian, C. X. Su and P. B. Armentrout, Collision-induced dissociation of Fe_n^+ (n = 2-19) with Xe: Bond energies, geometric structures, and dissociation pathways, *J. Chem. Phys.*, 1992, **97**(6), 4072–4083.
35 H. Yin, H. Tang, D. Wang, Y. Gao and Z. Tang, Facile Synthesis of Surfactant-Free Au Cluster/Graphene Hybrids for High-Performance Oxygen Reduction Reaction, *ACS Nano*, 2012, **6**(9), 8288–8297.
36 G. He, Y. Song, K. Liu, A. Walter, S. Chen and S. Chen, Oxygen Reduction Catalyzed by Platinum Nanoparticles Supported on Graphene Quantum Dots, *ACS Catal.*, 2013, **3**(5), 831–838.
37 M. Mavrikakis, B. Hammer and J. K. Nørskov, Effect of strain on the reactivity of metal surfaces, *Phys. Rev. Lett.*, 1998, **81**(13), 2819–2822.
38 S. Sakong and A. Gross, Dissociative adsorption of hydrogen on strained Cu surfaces, *Surf. Sci.*, 2003, **525**(1–3), 107–118.
39 G. S. Karlberg and G. Wahnstrom, Density-functional based modeling of the intermediate in the water production reaction on Pt(111), *Phys. Rev. Lett.*, 2004, **92**, 13.
40 C. J. Cramer, *Essentials of Computational Chemistry Theories and Models*, John Wiley & Sons, Ltd., West Sussex, England, 2nd edn, 2004, pp. 355–366.

